J. Mech. Phys. Solids Vol. 41, No. 12, pp. 1859–1886, 1993.
Printed in Great Britain.

0022–5096/93 $6.00 + 0.00

A GENERAL ANISOTROPIC YIELD CRITERION USING BOUNDS AND A TRANSFORMATION WEIGHTING TENSOR

A. P. KARAFILLIS and M. C. BOYCE

Department of Mechanical Engineering, Massachusetts Institute of Technology, Cambridge, MA 02139, U.S.A.

(*Received* 10 *February* 1993; *in revised form* 14 *June* 1993)

ABSTRACT

A GENERAL EXPRESSION for the yield surface of polycrystalline materials is developed. The proposed yield surface can describe both isotropic and anisotropic materials. The isotropic surface can be reduced to either the Tresca or von Mises surface if appropriate, or can be used to capture the yield behavior of materials (e.g. aluminum) which do not fall into either category. Anisotropy can be described by introducing a set of irreducible tensorial state variables. The introduced linear transformation is capable of describing different anisotropic states, including the most general anisotropy (triclinic) as opposed to existing criteria which describe only orthotropic materials. Also, it can successfully describe the variation of the plastic strain ratio (R-ratio), where polycrystalline plasticity models usually fail. A method for obtaining the material constants using only uniaxial test data is described and utilized for the special case of orthotropic anisotropy. Finally, the use of tensorial state variables together with the introduced mathematical formulation make the proposed yield function a very convenient tool for numerical implementation in finite element analysis.

INTRODUCTION

THE MODELING of the plastic behavior of metals is one of the most important aspects in the analysis of metal forming processes. There are primarily two different approaches to follow when describing the plasticity of polycrystalline materials. In the first approach, the TAYLOR (1938) polycrystalline plasticity model is used to describe both the initial yielding behavior and the subsequent evolution of anisotropy with deformation, ASARO and NEEDLEMAN (1985), DAWSON *et al.* (1992), KALIDINDI *et al.* (1992). However, the use of this formulation is very demanding in computational power when implemented in finite element analysis; see also DAWSON *et al.* (1992). Also, the Taylor model, while reasonably successful in fitting the anisotropic yield surface of FCC and BCC materials, has also been found to greatly overpredict the R-ratio (ratio of transverse to thickness strain in uniaxial tension) for some directions in anisotropic materials.

In the second approach, a phenomenological yield function is used to describe the initial yielding behavior whereas the plastic flow of the material is determined by the flow rule, where the plastic potential function is identical to the yield function. This yield function can be defined appropriately to describe the most important aspects of the

plastic behavior of both isotropic and initially anisotropic polycrystalline materials. In our work we will concentrate on the use of phenomenological yield theories which can be more flexible and efficient when implemented in finite element analysis (FEA), and which can more accurately predict failure and deformation processing behavior of initially anisotropic sheet metals.

The concepts of yield surface and plastic potential in stress space are among the most basic assumptions of the mathematical theory of plasticity. Several representations for the isotropic yield surface of polycrystalline materials have been proposed including those by TRESCA (1864), VON MISES (1913) and HOSFORD (1972). Anisotropic yield surfaces in stress space have also been proposed by many authors, the most well known being those of HILL (1950, 1979, 1990), BASSANI (1977), BUDIANSKY (1984), and BARLAT *et al.* (1989, 1991). In all of the yield theories listed above an associated flow rule was used and the yield surfaces were described as convex surfaces in stress space, as is also required by the maximum dissipation postulate. Also, yield surfaces for polycrystalline materials are generally taken to be pressure independent. In the present work we will be confined to yield surfaces which are homogeneous and convex in stress space. We will also assume an associated flow rule.

A generic formulation describing anisotropic yield surfaces must be able to describe the isotropic material as a special case. When the isotropic yield surface is recovered as a special case of the anisotropic yield function, it must have the properties of an isotropic function as described, for example, by GURTIN (1981). Also, it must be able to describe the anisotropy of any stress state of the material.

HILL's (1950) and BARLAT's (1991) anisotropic yield functions include all six components of the stress tensor. In both of these criteria a generalized framework of orthotropic symmetry is used. HILL's (1950) criterion takes the yield surface to be quadratic. However, experimental evidence (WOODTHROPE and PEARCE, 1970; STOUT *et al.*, 1983; MACEWEN *et al.*, 1992) and polycrystalline plasticity theories (BISHOP and HILL, 1951; HUTCHINSON, 1964) indicate that quadratic yield surfaces cannot successfully describe the yield surfaces of polycrystalline materials with an FCC or BCC microstructure. It has been shown by LIAN *et al.* (1989) that the necking behavior in biaxial tension is very sensitive to the shape of the yield locus and therefore a precise description of it is required. HERSHEY (1954) and HOSFORD (1972) have proposed a non-quadratic isotropic yield criterion to more accurately describe the yield surface of polycrystalline materials. The most important capability of this criterion is that it can approximately describe the yield surface of FCC materials as obtained by the Bishop–Hill model. However, this criterion is not flexible enough to describe any desired isotropic yield surface.

The criterion of BARLAT *et al.* (1991) is an extension of Hosford's criterion to also include orthotropic anisotropy. However, the BARLAT *et al.* (1991) criterion cannot be used for materials with symmetries other than the orthotropic symmetry (monoclinic, trigonal, asymmetric). Although the assumption of orthotropic symmetry is reasonable for thin rolled sheets, it also possesses a limitation for a generalized yield criterion, as orthotropic anisotropy is associated with only a limited set of strain paths. In general, many deformation histories may yield a totally asymmetric (triclinic) material.

In the present work we develop a new generic isotropic yield criterion for poly-

crystalline materials. This criterion is flexible and can describe different families of isotropic yield surfaces. An anisotropic yield criterion is presented as an extension of the isotropic criterion. The proposed anisotropic yield criterion uses a set of tensorial state variables to describe the anisotropy and therefore overcomes the defficiency of existing yield criteria which cannot describe materials which do not possess orthotropic symmetry. These tensorial state variables can be incorporated in a state representation of the material which describes both the stress and the anisotropic state and also provides the framework for later including evolution of anisotropy with plastic deformation.

A Generic Isotropic Yield Surface

We consider materials which exhibit pressure independent plasticity and initially consider isotropic materials. Therefore, the yield function is a function of only the principal values of the deviatoric Cauchy stress tensor **S**. Mendelson (1968) has shown the existence of bounds in an isotropic yield surface of a material with a fixed yield stress in uniaxial tension. These bounds are derived after symmetry and convexity considerations. The lower bound coincides with the limiting maximum shear stress yield surface as described by Tresca (1864), whereas the upper bound corresponds to a limiting value of the sum of the two greater diameters of Mohr's circles as mentioned by Hosford (1972). These two bounds of the yield surfaces of isotropic materials are depicted in Fig. 1. In the deviatoric plane section of the yield surface, the lower bound is inscribed in the von Mises yield circle which in turn is inscribed in the upper bound hexagon; see Fig. 1.

Isotropic yield surfaces lying between the bounds defined by the von Mises yield surface and the Tresca yield surface have been mathematically described by Hershey (1954) and Hosford (1972). Hosford's yield surface is a modification of the von

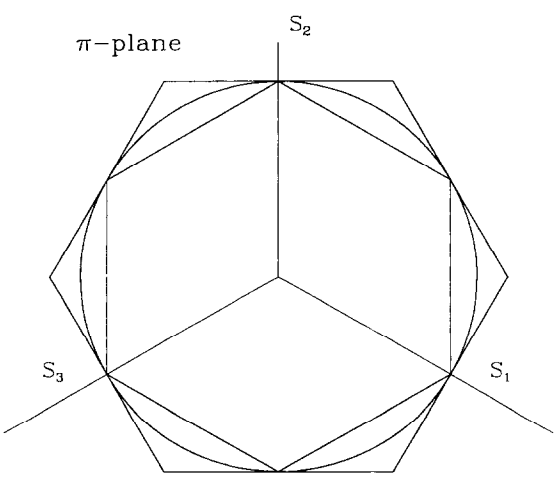

Fig. 1. The upper bound, the lower bound and the von Mises yield surface in the π-plane.

Mises mathematical description of a yield surface, where an exponent other than two is used in the following yield condition:

$$\Phi_1(\mathbf{S}(\boldsymbol{\sigma})) = (S_1 - S_2)^{2k} + (S_2 - S_3)^{2k} + (S_3 - S_1)^{2k} = 2Y^{2k} \tag{1}$$

where $S_i = S_i(\boldsymbol{\sigma})$ are the principal values of the deviatoric Cauchy stress tensor, and Y is the yield stress in uniaxial tension (a material property).

In the present work we will confine k to be an integer with values varying from $+1$ to $+\infty$. Thus, the exponent in (1) is always an even integer, thereby insuring equality of the tensile and compressive yield stress. When $k = 1$, (1) corresponds to the von Mises yield surface whereas when $k \to \infty$, (1) corresponds to the Tresca yield surface. Figure 2 shows sections of the yield surface of (1) in the σ_1 σ_2 (principal stress) space for different values of k.

In a similar way we can describe yield surfaces lying between the von Mises yield surface and the upper bound yield surface by using the following yield condition:

$$\Phi_2(\mathbf{S}(\boldsymbol{\sigma})) = S_1^{2k} + S_2^{2k} + S_3^{2k} = \frac{2^{2k}+2}{3^{2k}} Y^{2k}. \tag{2}$$

When $k = 1$ the yield surface of (2) corresponds to the von Mises yield surface whereas when $k \to \infty$ the upper bound yield surface is recovered. The σ_1-σ_2 section of the isotropic yield surface of (2) is shown in Fig. 3.

A generic isotropic yield surface should be able to describe all yield surfaces lying between the lower bound and the upper bound yield surface. The most plausible approach to such a generalized mathematical description can be obtained by mathematically mixing (1) and (2). We, therefore, establish the following yield condition:

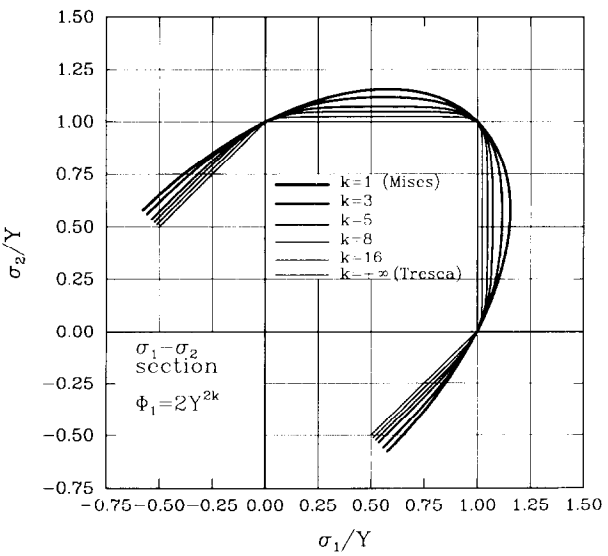

FIG. 2. Different isotropic yield surfaces between the von Mises yield surface and the lower bound (Tresca).

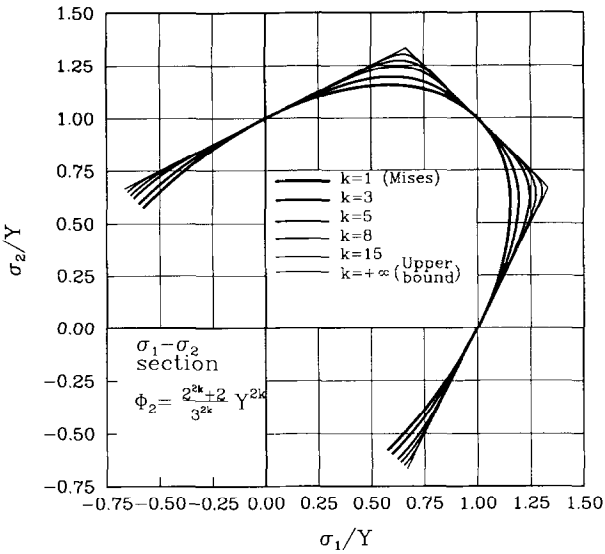

FIG. 3. Different isotropic yield surfaces between the von Mises yield surface and the upper bound.

$$\Phi(\mathbf{S}(\boldsymbol{\sigma})) = (1-c)\Phi_1(\mathbf{S}(\boldsymbol{\sigma})) + c\frac{3^{2k}}{2^{2k-1}+1}\Phi_2(\mathbf{S}(\boldsymbol{\sigma})) = 2Y^{2k} \tag{3}$$

where $c \in [0, 1]$. The yield surface of (3) lies between the bounds defined by (1) and (2) and preserves convexity.† As we increase the value of k the bounds described by (1) and (2) approach the lower and upper bound respectively. By varying the value of the mixing factor c, we create a family of yield surfaces which is swapping the space between the two bounds set by the selection of k. Yield surfaces for different values of c for $k = 15$ are depicted in Fig. 4, where we chose $k = 15$ to provide a nearly lower and upper bound representation as Φ_1 and Φ_2.

Equation (3) provides a general form for the yield surface spanning from lower to upper bound where the constant Y represents the yield stress in uniaxial tension. When using the isotropic yield function of (3) we fix the value of k to be high enough, e.g. 15, in order to describe the yield surface bounds, and then we find c simply by obtaining the yield stress in a different stress state, for example in plane strain or in shear (Method I). In an alternative approach, c and k can both be considered as material properties (i.e. k is not fixed to be large). In this case, k and c can be calculated to provide the best fit to an isotropic yield surface, as calculated experimentally or with polycrystalline plasticity considerations (Method II).

† Convexity of this proposed generic isotropic yield surface in the stress space must be assured. The yield surface is convex if the Hessian matrix Γ of $\Phi(\mathbf{S}(\boldsymbol{\sigma}))$ with respect to $\boldsymbol{\sigma}$ is positive semi-definite. The Hessian matrix is derived as: $\Gamma = \partial^2\Phi/\partial\boldsymbol{\sigma}^2$. RODIN and PARKS (1986) have established a criterion for determining the positive semi-definiteness of Γ. It can be shown that Γ is positive semi-definite when $2k > 1$.

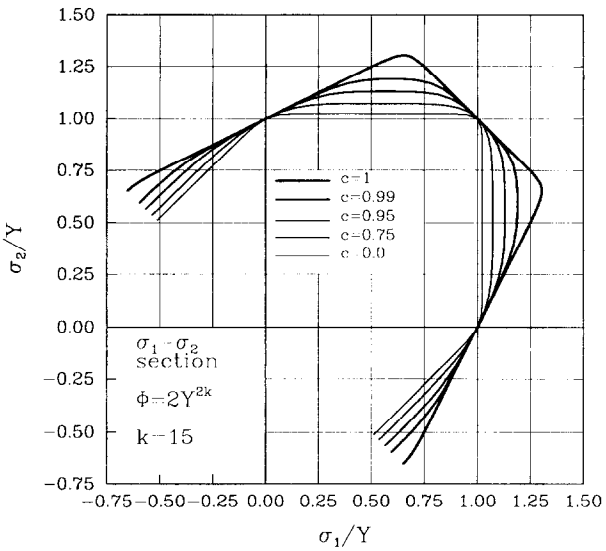

FIG. 4. Different isotropic yield surfaces between the lower bound (Tresca) and the upper bound.

AN ANISOTROPIC YIELD SURFACE

The yield function of (3) is an isotropic yield function. It also describes identical behavior in tension and compression. However, we would like to mathematically represent yield surfaces for anisotropic materials. We will again only consider convex and homogeneous yield surfaces.

BARLAT *et al.* (1991) used a linear transformation of the stress state of the anisotropic material to describe an anisotropic yield surface simply by multiplying all components of the Bishop–Hill stress tensor of the anisotropic material by a different constant. The obtained stress state was then used in HOSFORD's (1972) yield criterion.

In our development of an anisotropic yield function we will also consider a linear transformation of the actual stress tensor $\boldsymbol{\sigma}$ acting on the anisotropic material. This linear transformation "weights" the different components of the stress tensor of the anisotropic material in order to account for the anisotropy of the material. We call the transformed tensor the "isotropy plasticity equivalent (IPE) deviatoric stress tensor" and will be used as an argument in our isotropic function of (3). Therefore, for the case of an isotropic material, our linear transformation would yield the deviatoric stress tensor of the actual material stress state.

The generalized transformation of the stress state for an anisotropic material is schematically represented in Fig. 5. As also shown in Fig. 5, the concept of the "IPE material" is introduced. The "IPE stress transformation" introduced here is a transformation of the actual stress state of an anisotropic material to the corresponding stress state of an isotropic material whose yielding behavior is described by (3). We assign the same equivalent yield stress to both isotropic and anisotropic materials. We also set the plastic dissipation rate to be equal in both materials at the

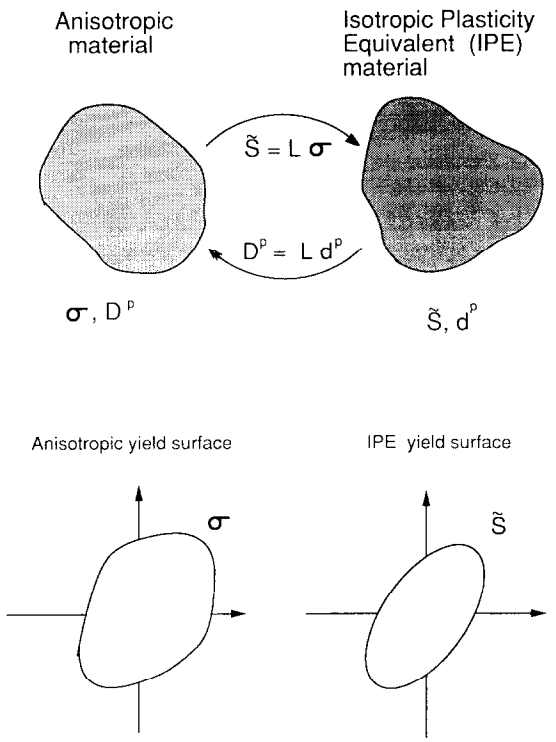

FIG. 5. The anisotropic material, the Isotropic Plasticity Equivalent (IPE) material and the IPE stress transformation.

time of yielding. Note that only the first plastic yield is considered in the developed framework of the transformation, i.e. ongoing evolution in anisotropy with further plastic strain is currently neglected.

The linear transformation of the stress state of the anisotropic material can be effected by multiplicatively operating on the stress tensor $\boldsymbol{\sigma}$ with fourth order tensorial operator. Such a transformation is an affine transformation and therefore preserves the convexity of the yield surface (EGGLESTON, 1969) as also noted by BARLAT *et al.* (1991). We will show that the tensorial multiplicative operator used in our "IPE stress transformation" must exhibit some internal symmetries and it must also be traceless. Fourth order tensorial stress concentration operators have also been considered by DVORAK and BAHEI-EL-DIN (1982) in conjunction with the von Mises yield criterion for anisotropic composite materials. Also, fourth order tensors have been used in different formulations of quadratic yield criteria by SHIH and LEE (1978), EISENBERG and YEN (1984), and VOYADJIS and FOROOZESH (1990). As shown by ONAT (1984) and developed in detail in Appendix 1, fourth order traceless tensors with the internal symmetries required by our transformation are composed of a set of irreducible tensorial variables (one scalar, a second order tensor and a fourth order tensor). With the use of group theory (BACKUS, 1970) it is shown that the fourth order irreducible

tensorial component of $\mathbf{L}$ can be associated with material symmetries which range from the lowest level of the triclinic symmetry to the highest level of full symmetry. Therefore, the use of the fourth order tensor as a linear multiplicative operator provides a tool for representing different degrees of material symmetry and provides a potential for representation of any anisotropic state of the material.

The "IPE stress transformation" operates as

$$\tilde{\mathbf{S}} = \mathbf{L}\boldsymbol{\sigma} \tag{4}$$

where $\mathbf{L}$ is the fourth order tensorial operator, $\tilde{\mathbf{S}}$ is the IPE stress tensor, $\boldsymbol{\sigma}$ the actual stress tensor of the anisotropic material. The yield condition of the anisotropic material is

$$\Phi(\tilde{\mathbf{S}}) = 2Y^2 \tag{5}$$

where $\tilde{\mathbf{S}}$ replaces $\mathbf{S}$ in our generic isotropic yield function of (3) earlier and Y is the average yield stress in uniaxial tension obtained experimentally. In order to establish the form and properties of the introduced tensorial operator we consider the stress tensor and the material symmetries. First, by the symmetry of $\boldsymbol{\sigma}$ and $\tilde{\mathbf{S}}$ we have

$$L_{ijkl} = L_{jikl} = L_{jilk}. \tag{6}$$

As also discussed in Appendix 1, we require $\mathbf{L}$ to also exhibit the symmetry

$$L_{ijkl} = L_{klij}. \tag{7}$$

As mentioned above, yielding in the anisotropic material is also pressure independent. Therefore, the values of the components of the "IPE deviatoric stress tensor" should be independent of the hydrostatic pressure component of $\boldsymbol{\sigma}$. We can mathematically express this condition as a property of the fourth order tensorial operator $\mathbf{L}$:

$$L_{ijkk} = 0 \tag{8}$$

where the standard summation rules apply.

The symmetries expressed by (6) and (7) together with the constraint of (8) render $\mathbf{L}$ a traceless partially symmetric fourth order tensor. We can now derive the population of the independent scalar components of $\mathbf{L}$ after the constraints of (6)–(8) for different degrees of material symmetry. In Table 1 the rotations which leave $\mathbf{L}$ invariant and the corresponding number of independent components of the tensorial operator are tabulated, where $\mathbf{R}_i^{\phi}$ denotes rotation about the i-axis by the angle ϕ. Also, any

TABLE 1

Material symmetry	Rotations which leave $\mathbf{L}$ invariant	Number of independent elements of $\mathbf{L}$
Triclinic	No rotation	15
Monoclinic	$\mathbf{R}_3^{\pi}$	8
Orthotropic	$\mathbf{R}_1^{\pi}, \mathbf{R}_2^{\pi}$	6
Trigonal	$\mathbf{R}_3^{2\pi/3}, \mathbf{R}_1^{\pi}$	4
Tetragonal	$\mathbf{R}_3^{\pi/2}, \mathbf{R}_1^{\pi}$	4
Transversely isotropic	all $\mathbf{R}_3^{\phi}, \mathbf{R}_1^{\pi}$	3
Cubic	$\mathbf{R}_1^{\pi/2}, \mathbf{R}_2^{\pi/2}, \mathbf{R}_3^{\pi/2}$	2
Isotropic	All rotations	1

rotation which is derived as the product of the rotations tabulated in Table 1 would leave **L** invariant. We see that for isotropic symmetry only one constant can completely describe the tensorial operator whereas in the case of triclinic symmetry, 15 components are needed to describe the operator. In Appendix 1 the three state variables that compose **L** are shown: a scalar a, a second order traceless and symmetric tensor **A**, and a fourth order traceless and symmetric tensor **C**, as shown in the following equation:

$$L_{ijkl} = a\delta_{ij}\delta_{kl} - \tfrac{3}{2}a(\delta_{ik}\delta_{jl}+\delta_{il}\delta_{jk}) + \delta_{ij}A_{kl} + A_{ij}\delta_{kl} - \tfrac{3}{4}(\delta_{ik}A_{jl}+\delta_{il}A_{jk}+\delta_{jk}A_{il}+\delta_{jl}A_{ik}) + C_{ijkl}. \quad (9)$$

These variables in combination with the stress tensor $\boldsymbol{\sigma}$ and the stress magnitude Y can be used to represent the state of the material, see Appendix 1. The tensorial variables in this representation can be rotated with the tensor rotation rule when the reference frame is rotated and still be compatible to the IPE stress transformation as both the anisotropic and the equivalent isotropic material are attached to the same reference frame. Also evolution equations for the developed tensorial state variables may provide a tool for the description of the evolution of the anisotropy of a material subject to mechanical processing and/or thermal treatment. However, the validity of this hypothesis requires further investigation.

The equality of the plastic dissipation rate of the general anisotropic material and the equivalent isotropic material can now be considered. It is

$$\dot{W} = \boldsymbol{\sigma}\cdot\mathbf{D}^{\mathrm{p}} = \tilde{\mathbf{S}}\cdot\mathbf{d}^{\mathrm{p}} = Y\dot{\bar{\varepsilon}}^{\mathrm{p}} \quad (10)$$

where $\dot{W}$ is the plastic dissipation rate, $\mathbf{D}^{\mathrm{p}}$ is the symmetric part of the plastic velocity gradient tensor (plastic stretching) at the moment of the first yield of the anisotropic material, whereas $\mathbf{d}^{\mathrm{p}}$ is the work conjugate of the IPE deviatoric stress $\tilde{\mathbf{S}}$. We assume an associated flow rule and therefore the yield function can also be used as a plastic potential. If λ is a scalar such that

$$\mathbf{d}^{\mathrm{p}} = \lambda\frac{\partial\Phi}{\partial\tilde{\mathbf{S}}} \quad (11)$$

then by using the homogeneity of Φ, $(\tilde{\mathbf{S}}\cdot(\partial\Phi/\partial\tilde{\mathbf{S}}) = 2k\Phi)$, combined with (10) we obtain

$$\dot{W} = \lambda\tilde{\mathbf{S}}\cdot\frac{\partial\Phi}{\partial\tilde{\mathbf{S}}} = 4\lambda k Y^{2k}. \quad (12)$$

Therefore

$$\lambda = \frac{\dot{W}}{4kY^{2k}} \quad (13)$$

and

$$\mathbf{d}^{\mathrm{p}} = \frac{\dot{W}}{4kY^{2k}}\frac{\partial\Phi}{\partial\tilde{\mathbf{S}}} = \frac{\dot{W}}{4kY^{2k}}\mathbf{Q}^{\mathrm{T}}\frac{\partial\Phi}{\partial\boldsymbol{\Lambda}}\mathbf{Q} \quad (14)$$

where $\mathbf{Q}$ is the rotation matrix whose rows are the eigenvectors of $\tilde{\mathbf{S}}$, and $\mathbf{\Lambda}$ is the principal tensor of $\tilde{\mathbf{S}}$ obtained as

$$\mathbf{\Lambda} = \sum_{i}^{3} S_i \mathbf{v}_i \otimes \mathbf{v}_i \tag{15}$$

where $\mathbf{v}_i$ are the eigenvectors of $\tilde{\mathbf{S}}$.

Also, from the flow normality rule and by using the symmetry of $\mathbf{L}$ expressed by (8) we obtain

$$\mathbf{D}^{\mathrm{p}} = \frac{\dot{W}}{4k\,Y^{2k}} \frac{\partial \Phi}{\partial \boldsymbol{\sigma}} = \frac{\dot{W}}{4k\,Y^{2k}} \mathbf{L} \frac{\partial \Phi}{\partial \tilde{\mathbf{S}}} = \mathbf{L}\mathbf{d}^{\mathrm{p}}. \tag{16}$$

Equation (16) constitutes the flow rule for the anisotropic material as derived from the plastic potential proposed in the present work. Operationally, we will determine the plastic strain ratios or R-values using (16).

The "Backstress" State Variable

The isotropic and anisotropic yield functions presented in the above sections assume that the yield stress in tension is equal to the yield stress in compression in all directions. However, it has been observed that plastic deformation in the reverse direction typically initates at a lower yield stress ("Bauschinger" effect). Also, differences between the tensile and the compressive yield stress can be associated with crystallographic phenomena (twinning) in HCP materials, see also Backofen (1972). The proposed yield surface is not capable of describing the "Bauschinger" phenomenon. However, we can further expand (5) as

$$\tilde{\mathbf{S}} = \mathbf{L}(\boldsymbol{\sigma} - \mathbf{B}) \tag{17}$$

where $\mathbf{B}$ is an irreducible symmetric and traceless tensorial state variable of second order, which results in different yield stresses in tension and compression. The flow rule in this case remains as given by (16). The "backstress" $\mathbf{B}$ can be included in the set of irreducible tensorial variables which describe the state of the material, see also Appendix 1.

Procedures for the Evaluation of the Yield Surface

We will concentrate now on the procedures for the estimation of the yield surface of anisotropic materials based on experimental material data.

Isotropic material

We consider now the two different methods for the calculation of an isotropic yield surface. In the first method (Method I) we fix k to a high enough value ($k = 15$) to

provide a nearly lower and upper representation of Φ_1 and Φ_2. Then we modify c until a desired value of the yield stress in plane strain tension is reached. This value can be obtained either experimentally or by using polycrystalline plasticity considerations. However, as it is difficult to obtain experimental results for the isotropic state of commercially available thin rolled materials, we used the Bishop–Hill method as it is implemented in the popLA code, developed by KALLEND *et al.* (1989), where a fully symmetric Sample Orientation Distribution Function was used to calculate the average macroscopic plane strain yield stress. Also, the restricted glide assumption was used for FCC materials and the pencil glide assumption was used for BCC materials. The computed Bishop–Hill surfaces are shown in Fig. 6(a). The values of c obtained using this method are tabulated in Table 2. Also, the sections of the yield surfaces obtained in the σ_1–σ_2 domain are virtually identical to those obtained with popLA, compare Figs 6(a) and 6(b).

In the second method (Method II) we modified both k and c until we obtained a precise description of the Bishop–Hill yield surface. In order to graphically represent the detailed features of the shape of the yield surface, we depicted it by using LODE's (1926) variables, $\nu = 3(D_{\max}+D_{\min})/(D_{\max}-D_{\min})$ and $\alpha = (S_{\max}-S_{\min})/Y$. $D_{\max}$ and $D_{\min}$ are respectively the maximum and minimum principal components of the plastic stretching rate tensor as derived from the flow normality rule whereas $S_{\max}$ and $S_{\min}$ are respectively the maximum and minimum principal components of the deviatoric stress tensor. Correlation between these variables describes completely and in detail all the particular features of the shape of the isotropic yield surface. The exponent k and the mixing coefficient c of the isotropic function of (3) were determined to provide a best fit to the α–ν diagram as derived from polycrystalline plasticity considerations, see Fig. 7. The values of these parameters for the different cell-structures considered here are tabulated in Table 2. The obtained yield surfaces in the σ_1–σ_2 domain were almost identical with the ones obtained by popLA and Method I, see also Figs 6(a) and (b), where the largest differences occur near corner-like regions. However, some differences still exist in both the σ_1–σ_2 domain and the α–ν domain and the yield surface obtained by Method II provides a better description of the Bishop–Hill yield surface. These differences may drastically affect the Forming Limit Diagram (FLD) of the isotropic material, as also mentioned by LIAN *et al.* (1989), because it is the shape of the yield surface and its corresponding normal which determines the straining and thinning behavior of the sheet. Therefore the appropriate method and combination of coefficients to describe the yield surface of the isotropic material should be selected by comparison with experimental measurements of the yield surface and/or measurements of the FLD.

Prior to comparing the model predictions and capabilities with experimental data, we first show the general anisotropic features of different symmetry aspects of the model.

Anisotropic material

In order to describe the plasticity of an anisotropic material we must estimate the values of the independent components of the anisotropy tensorial operator by using experimental data. We will concentrate on thin rolled metallic materials which usually

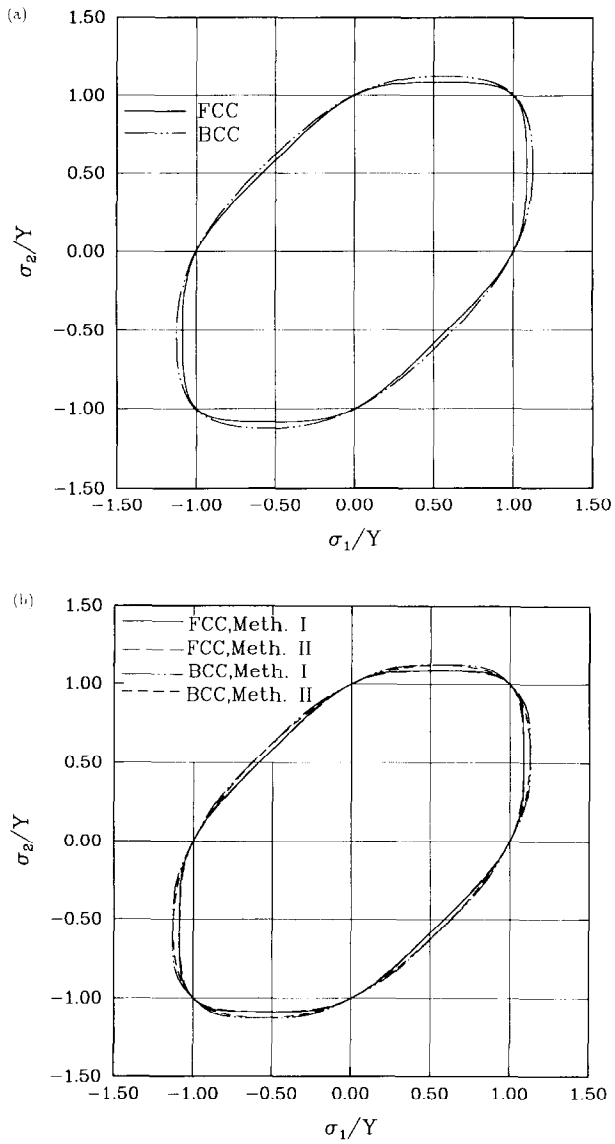

FIG. 6. (a) Isotropic yield surfaces for FCC (restricted glide) and BCC (pencil glide) materials obtained by popLA. (b) Isotropic yield surfaces as obtained by using Method I and Method II.

exhibit orthotropic symmetry as a result of the geometry of the rolling process and the small thickness of the sheet. In Appendix 2 we show the form of the tensorial operator when the orthotropic axes of the material are aligned with the reference system coordinate axes. The IPE function of the IPE material is determined by using Method I, where $k = 15$ and c is determined in order to provide the best fit to the experimental data due to its important effect on the shape of the yield surface and the

TABLE 2. *Isotropic material*

Method I			Method II		
Slip system	k	c	Slip system	*k*	*c*
FCC (restricted glide)	15	0.835	FCC (restricted glide)	6	0.3
BCC (pencil glide)	15	0.948	BCC (pencil glide)	3	0.17

R-ratio, see also Appendix 2. Alternatively we could use Method II and determine both k and c in order to control the shape of the yield surface to a greater extent. However, for the materials examined here we found Method I a very good approximation. Also, the procedure followed to calculate the independent components of the tensorial operator is developed in detail in Appendix 2, where three tension tests are required to completely determine **L** and c. These tests are uniaxial tests of specimens cut at 0°, 45° and 90° with respect to the rolling direction.

SPECIAL CASES OF ANISOTROPY

In order to demonstrate the ability of the proposed method to describe the first yield of materials with different symmetries we consider two different cases.

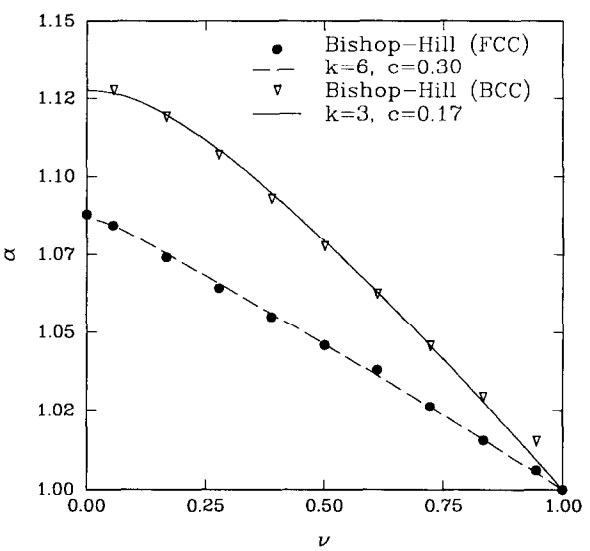

FIG. 7. Different isotropic yield surfaces in the α–ν domain.

Cubic symmetry

We consider a material possessing properties which remain invariant under rotations of 90° about all three orthonormal axes. Thus, the IPE transformation tensor **L** will have to remain invariant under these rotations. By using this property and (6)–(8), we can derive that the non-zero components of **L** will follow the relations:

$$L_{1111} = L_{2222} = L_{3333}$$

$$L_{1122} = L_{1133} = L_{2233} = -\frac{L_{1111}}{2}$$

$$L_{1212} = L_{2323} = L_{3131}. \tag{18}$$

It is also required by symmetry considerations that $\mathbf{B} = \mathbf{0}$. Therefore, as also tabulated in Table 1, only L_{1111} and L_{1212}, i.e. two scalars, are necessary to describe the IPE transformation tensor when the material exhibits cubic symmetry. In Fig. 8 we plot the yield stress for different angles of rotation about the 3-axis where the ratio of $\beta = ((4L_{1212}/3L_{1111}) - 1)$ was used as an anisotropy parameter. The parameter β provides a measure for the deviation of the material from the isotropic behavior. When $\beta = 0$ the material is isotropic and when the absolute value of β increases, the cubic anisotropy becomes stronger. The yield stress was calculated by using the isotropic yield function of (3), in conjunction with the IPE transformation as also indicated in (5). For example purposes, the values of c and k were the ones which correspond to isotropic FCC materials as tabulated in Table 2 (Method I). We see that we can successfully describe the cubic symmetry as the yield stress remains identical under rotations of 90°. We also note the presence of four peaks in the yield

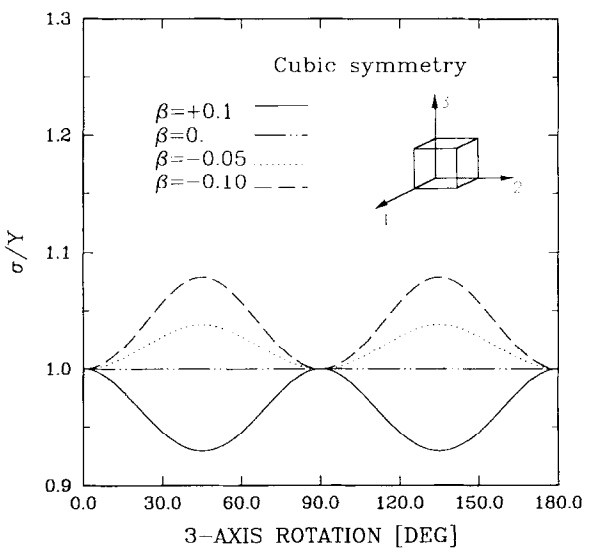

FIG. 8. Distribution of the uniaxial yield stress in different angles about the 3-axis for a material with cubic symmetry. The parameter β indicates degree of anisotropy.

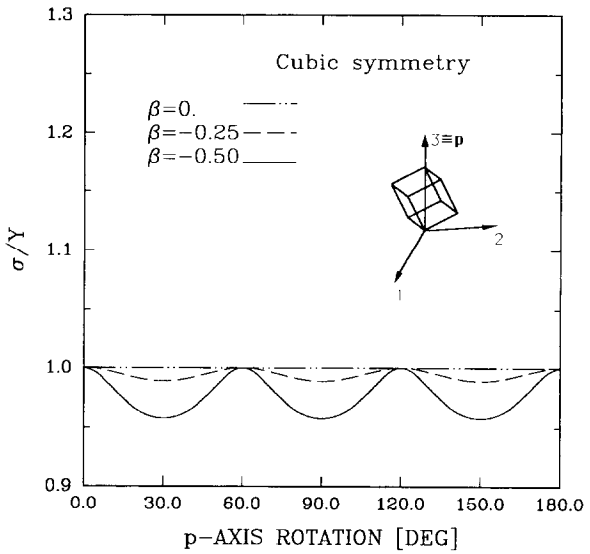

FIG. 9. Distribution of the uniaxial yield stress in different angles about the **p**-axis for a material with cubic symmetry. The parameter β indicates degree of anisotropy.

stress which corresponds to the presence of four "ears" during the cup forming and/or deep drawing of most aluminum sheets. Also, as shown in Fig. 8, the location of the ears can change when the sign of β alternates. Also, in Fig. 9 we depict the yield stress for different angles of rotation about the **p**-axis, where $\mathbf{p} = (\mathbf{e}_1+\mathbf{e}_2+\mathbf{e}_3)/\sqrt{3}$ and $\mathbf{e}_i$, $i = 1, 2, 3$ are the unit vectors along the 1, 2, 3 axis respectively. We note that in this case we observe six-peaks in the yield stress variation along a rotation of 180° around the **p**-axis. This phenomenon indicates the existence of six-ears in a cup formation of a thin disk made of a material that exhibits cubic symmetry and for which the **p**-axis is normal to the plane of the disk. This behavior cannot be described by quadratic yield surfaces, see also HILL (1950).

We note here that six-ears in cup forming of single crystal sheets were observed by TUCKER (1961) for cubic crystals having their **p**-axis normal to the sheet. Therefore, although the anisotropic yield surface proposed here was not constructed with the intention of describing the plastic behavior of single crystals, we see that it can very successfully describe the way in which the symmetries of the material and associated orientations can affect its plastic behavior.

Trigonal symmetry

In this case, the material properties remain invariant for rotations of 120° about the 3-axis and for the reflection with respect to the 1–2 plane. Although this case is not the result of a specific forming process, we present it here in order to illustrate how different material symmetries may affect the material's plastic behavior. By using this property we obtain the following relations for the non-zero components of **L**:

$$
\begin{aligned}
L_{1111} &= L_{2222} \\
L_{1122} &= \frac{L_{3333} - 2L_{1111}}{2} \\
L_{1133} &= L_{2233} = -\frac{L_{3333}}{2} \\
L_{1123} &= -L_{2223} \\
L_{2323} &= L_{1313} \\
L_{1213} &= L_{1123} \\
L_{1212} &= \frac{L_{1111} - L_{1122}}{2}.
\end{aligned} \tag{19}
$$

It is also required by symmetry considerations that $\mathbf{B} = \mathbf{0}$. From (18) it can be seen that only L_{1111}, L_{1123}, L_{3333} and L_{2323} are necessary to fully describe $\mathbf{L}$.

In Fig. 10, we depict the variation of the yield stress as a function of the rotation about the 3-axis. For example purposes, the values of c and k in function Φ were obtained to be the ones which correspond to FCC materials as tabulated in Table 2 (Method I). We assumed that $L_{1111} = L_{2222} = L_{3333} = \frac{4}{3}L_{1212}$ (same as for the isotropic material), whereas the ratio $\zeta = L_{1123}/L_{1111}$ was used as the trigonal anisotropy parameter, where large values of ζ indicate trigonal anisotropy. It can be seen in Fig. 10 that peaks in the yield stress are 60° apart, indicating the formation of six-ears in a cylindrical cup-forming operation.

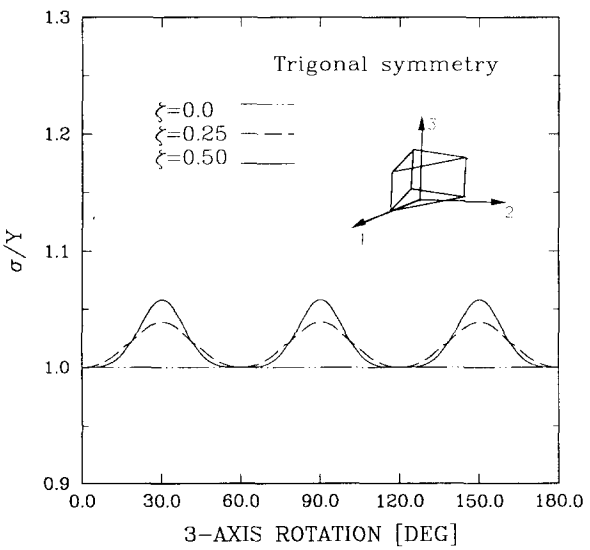

FIG. 10. Distribution of the uniaxial yield stress in different angles about the 3-axis for a material with trigonal symmetry. The parameter ζ indicates degree of anisotropy.

The case of trigonal anisotropy shows that the introduction of components of **L** which destroy its orthotropic symmetry can affect the anisotropic behavior of the material by changing the amount of ears observed in a cup-forming operation.

Comparison with Experiments

We now use the proposed yield surface to describe the anisotropy of thin rolled aluminum alloys, where orthotropic symmetry is assumed. The yield function of the IPE material is determined following Method I, where k is fixed to a high value to approximately describe the upper and lower bound ($k = 15$), whereas the mixing factor c is modified to provide the best agreement with experiments due to its important effect on the shape of the yield surface and the distribution of the R-ratio, see also Appendix 2. This method was found very effective for all the examined aluminum alloys. The procedure to calculate the independent parameters of **L** and the value of c is developed in Appendix 2. In this procedure, only the R-ratio and average yield stress from three tension tests in three different directions (0°, 45° and 90°) are required to determine **L**, the yield stress distribution and yield surface can then be predicted. The value of the mixing coefficient c of the IPE yield surface can be modified to optimize the prediction of the IPE yield surface. Alternatively, we can use Method II to describe the IPE yield surface and modify both k and c to optimize the predictions of the yield stress distribution and/or the yield surface.

Two different materials were considered: the H19 can stock aluminum and the 2008-T4 aluminum. Results concerning the anisotropic behavior of the H19 aluminum at initial yield were obtained from MacEwen *et al.* (1992). For this material we assumed that $\mathbf{B} = \mathbf{0}$. In their work, MacEwen *et al.* measured the experimental data which are necessary to determine the anisotropy of the material. Therefore we were able to completely determine **L**, assuming orthotropic anisotropy. This determined IPE transformation tensor **L** was used in conjunction with the isotropic function Φ. The values of all of the corresponding coefficients are tabulated in Table 3. The variation of the R-ratio as a function of the angle from the rolling direction is depicted in Fig. 11(a). The experimental values of the R-ratio at 0°, 45° and 90° were the only data used to determine **L** and therefore there was very good agreement between theory and experiment, as also shown in Fig. 11(a). We can now *predict* the variation of the tensile yield stress is uniaxial tension with respect to the angle from the rolling

Table 3. *Material constants*

Material	k	c	C	α_1	α_2	γ_3	**B**
H-19 can stock	15	0.36	0.644	0.931	0.989	0.728	**0**
2008-T4	15	0.81	0.559	1.103	1.120	0.730	**0**
$\mathbf{B} = \mathbf{0}$							
2008-T4	15	0.3	0.575	1.083	1.057	0.762	$B_{11} = 0.012Y$
$\mathbf{B} \neq \mathbf{0}$							$B_{22} = -0.018Y$
							$B_{33} = 0.006Y$

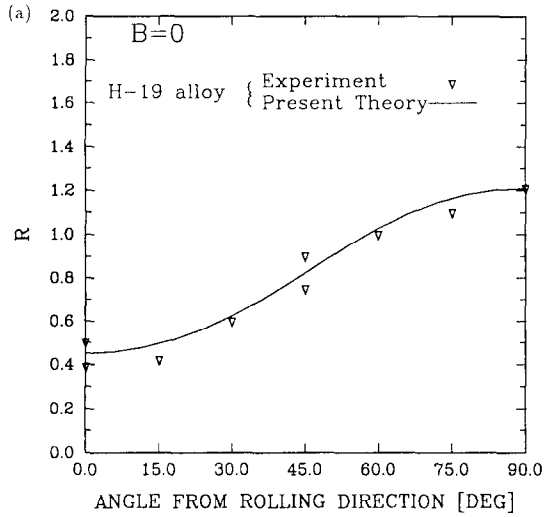

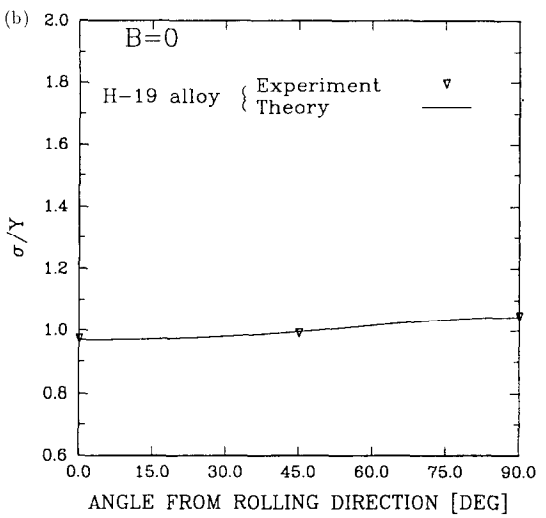

FIG. 11. (a) The distribution of the R-ratio with respect to the angle with the rolling direction for the H-19 can stock alloy. Experimental results were obtained by MACEWEN *et al.* (1992). (b) The distribution of the yield stress in uniaxial tension with respect to the angle with the rolling direction for the H-19 alloy. Experimental results were obtained by MACEWEN *et al.* (1992).

direction. All yield stress measurements were obtained at 0.1% offset. Also, error bars for the yield stress mesurements were not reported. In Fig. 11(b), predictions and experimental values of the yield stress for different angles to the rolling direction are depicted, where excellent agreement between theory and experiment is observed. All stresses in Fig. 11(b) are normalized with the experimental average tensile yield stress.

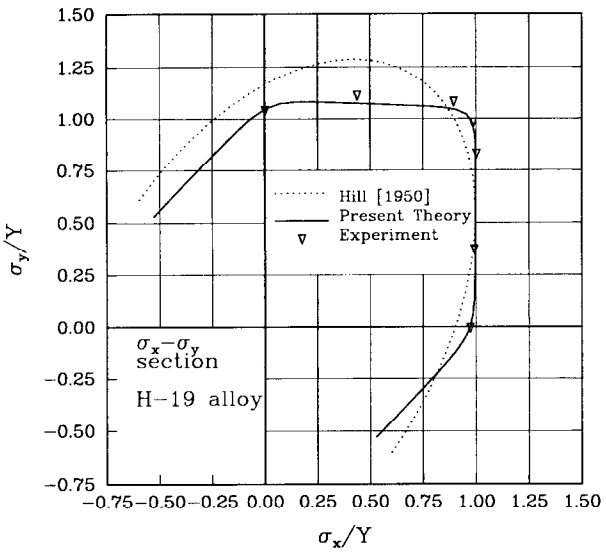

FIG. 12. The yield surface of the H-19 can stock aluminum alloy in the σ_x, σ_y domain. Experimental results were obtained by MACEWEN *et al.* (1992).

We see that our anisotropic function which was determined by R-ratio measurements in different stress states can also satisfactorily predict the variation of the yield stress in different directions, thereby indicating the effectiveness of the yield function. Also, in Fig. 12 the projection of the yield surface in the σ_x–σ_y plane is depicted, where x is the rolling direction and y the transverse direction. The stresses in this graph are normalized with the experimental average tensile yield stress. Again, we see the excellent agreement between the prediction with the present theory and the biaxial experimental results as opposed to the predictions with HILL's (1950) quadratic criterion.

Similar results and conclusions are obtained for the 2008-T4 aluminum. For this material, experimental data were obtained by LEGE *et al.* (1989). The yield stress was measured in 0.2% offset with a reproducibility of the order of 4%, whereas the reproducibility in the measurements of the R-ratio was of the order of 1%. In a first approach we assume that $\mathbf{B} = \mathbf{0}$ for this material. The strain ratio data in different directions were used in order to calculate $\mathbf{L}$ by following the procedures described in Appendix 2. The results are shown in Fig. 13(a). We see again that our yield function successfully describes the variation of the yield stress and the R-ratio in the different directions. The results obtained by using the proposed yield function and the suggested procedures for determining $\mathbf{L}$ can be compared with the results obtained by using Barlat's yield criterion as presented by BARLAT *et al.* (1991) for the same material, see Fig. 13(a). Before any comparisons are made, we note that Barlat's criterion can be recovered as a special case of the proposed criterion, if we set $c = 0$ in the function of (3). It can also be shown that the coefficients of Barlat's yield function can be obtained as linear combinations of the independent components of $\mathbf{L}$. We see that the

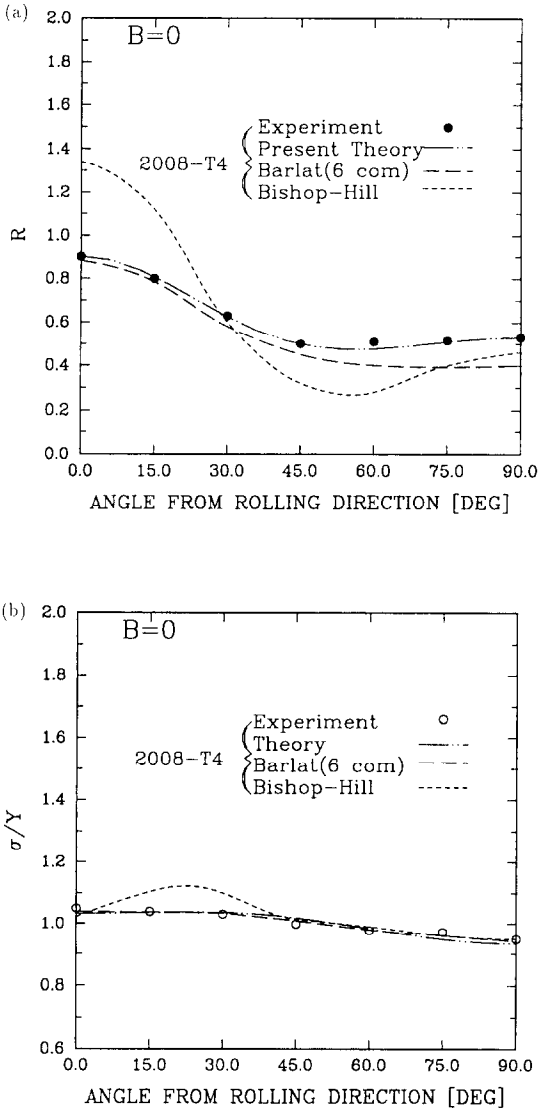

FIG. 13. (a) The distribution of the R-ratio with respect to the angle with the rolling direction for the 2008-T4 aluminum alloy. Experimental results by LEGE *et al.* (1989). The Bishop Hill distribution was obtained by LEGE *et al.* (1989). (b) The distribution of the yield stress in uniaxial tension with respect to the angle with the rolling direction for the 2008-T4 aluminum alloy. The experimental results and the Bishop Hill distribution were obtained by LEGE *et al.* (1989).

proposed yield function and the procedures to estimate its parameters can better describe the variation of the R-ratio, see Fig. 13(a), and correctly predict the yield stress distribution, see Fig. 13(b). Also in Figs 13(a) and (b) we show the variation of the R-ratio and the tensile yield stress respectively as predicted in the work of LEGE

et al. (1989) by using crystallographic distribution data in combination with the Bishop–Hill method, where we see that the polycrystalline plasticity is not very successful in describing the distribution of the R-ratio and the tensile yield stress as opposed to the proposed yield function. We also emphasize that the ability to accurately predict the R-ratio and its anisotropy is important in the material characterization for forming simulations as this greatly influences the predicted thinning of the sheet during a process.

In Fig. 14(a) we show the distribution of the yield stress for the 2008-T4 aluminum alloy when the "backstress" tensorial state variable is also invoked. The "backstress" variable was introduced in order to describe the difference of the tensile and compressive yield stress as obtained in the experiments of LEGE *et al.* (1989). Orthotropic symmetry implies that all of the non-diagonal components of **B** are zero. The components of **B** for this material are shown in Table 3. The obtained distributions of the yield stress compare well with the experimental data. Also, the obtained distribution of the R-ratio was again in excellent agreement with the experimental data, see Fig. 14(b). The predicted yield surfaces with and without the "backstress" tensorial variable are shown in Fig. 15. The obtained yield surface accounts for the different yield stresses in tension and compression as found by the experimental data. Furthermore, we note that the important effect of the introduction of a "small" backstress **B** on the shape of the yield surface in order to yield the same distribution of the R-ratio. We observe that by introducing **B** we also significantly increase the yield stress in the biaxial tension regime, see Fig. 15. This observation suggests that the "anomalous" behavior of aluminum, as described by WOODTHROPE and PEARCE (1970), and STOUT *et al.* (1983) (high biaxial yield stress combined with low R-ratio) could be partially attributed to the existence of Bauschinger phenomena. HILL's (1979) yield function was introduced to represent a yield surface which could describe the anomalous behavior of aluminum but without including any "Bauschinger" phenomena.

CONCLUSIONS

A generalized yield criterion using bounds and a transformation weighting tensor has been developed. The proposed yield function can describe both isotropic and anisotropic materials. The anisotropy is described by a linear transformation of the stresses. This linear transformation is effected by the use of a set of tensorial variables which can describe both anisotropy and Bauschinger phenomena. The proposed yield criterion is capable of describing different states of material symmetry, including the most generalized case of the totally asymmetric material, in combination with a non-quadratic yield criterion. The yield criterion was found to be in good agreement with experimental results available in the literature for a variety of materials. For the special case of orthotropic materials, and if we neglect Bauschinger effects, only three tension tests are required to fully determine the anisotropy of the material. Also the use of tensorial variables in combination with the compact form of the proposed non-quadratic yield criterion render the proposed yield function very convenient when implemented in computational procedures and also provides a framework for later, including evolving anisotropy.

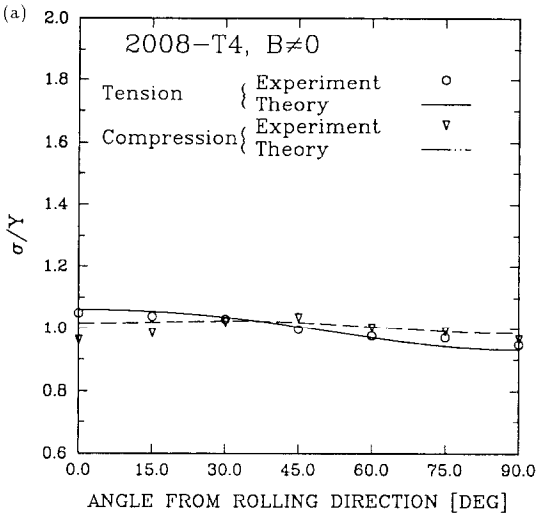

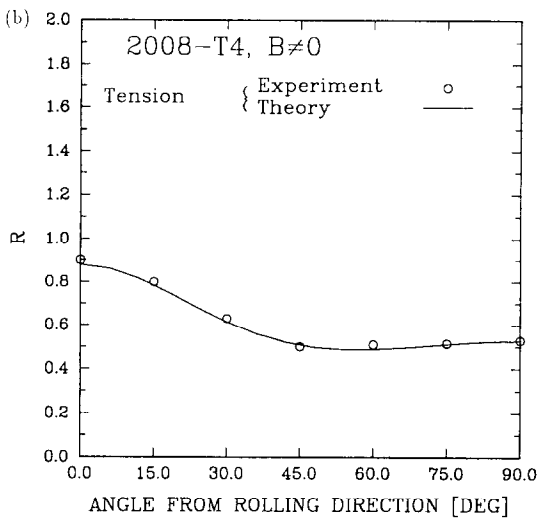

FIG. 14. (a) The distribution of the tensile and compressive yield stress with respect to the angle with the rolling direction for the 2008-T4 aluminum alloy. Experimental results were obtained by LEGE *et al.* (1989). (b) Theoretical and experimental distribution for the R-ratio for the 2008-T4 alloy. The theoretical distribution was obtained with $\mathbf{B} \neq \mathbf{0}$. Experimental results by LEGE *et al.* (1989).

ACKNOWLEDGEMENTS

This research has been funded by the NSF-DDM-9202362 grant, Division of Manufacturing and Design. Additional funding to APK was provided by the Greek Orthodox Church of North and South America. Also, input from discussions with Professors D. M. Parks and F. A. McClintock is greatly appreciated.

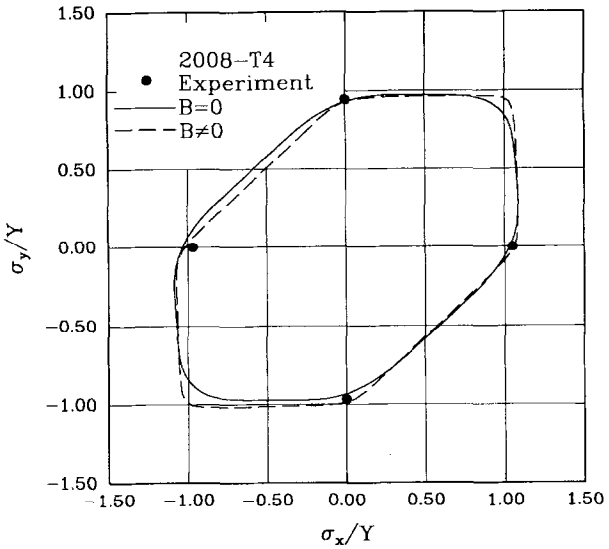

FIG. 15. The projection of the yield surface in the σ_x, σ_y domain for the 2008-T4 material. Experimental results were obtained by LEGE *et al.* (1989).

REFERENCES

ASARO, R. J. and NEEDLEMAN, A. (1985) Texture development and strain hardening in rate dependent polycrystals. *Acta Metall.* **33,** 923.

BACKOFEN, W. A. (1972) *Deformation Processing.* Addison-Wesley, Reading, MA.

BACKUS, G. (1970) A geometric picture of anisotropic elastic tensors. *Rev. Geophys. Space Phys.* **8,** 633.

BARLAT, F., LEGE, D. J. and BREM, J. C. (1991) A six-component yield function for anisotropic materials. *Int. J. Plasticity* **7,** 693.

BARLAT, F. and LIAN, J. (1989) Plastic behavior and stretchability of sheet metals. Part I: A yield function for orthotropic sheet under plane stress conditions. *Int. J. Plasticity* **5,** 51.

BASSANI, J. L. (1977) Yield characterization of metals with transversely isotropic plastic properties. *Int. J. Mech. Sci.* **19,** 651.

BISHOP, J. F. W. and HILL, R. (1951) A theory of the plastic distortion of a polycrystalline aggregate under combined stresses. *Phil. Mag.* **42,** 414.

BUDIANSKY, B. (1984) Anisotropic plasticity of plane-isotropic sheet. *Mechanics of Material Behavior* (ed. G. J. DVORAK and R. T. SHIELD), p. 15. Elsevier, Amsterdam.

DAWSON, P. R. BEAUDOIN, A. J. and MATHUR, K. K. (1992) Simulation of deformation-induced texture in metal forming. *NUMIFORM '92* (ed. J.-L. CHENOT *et al.*), p. 25. Balkema, Sophia-Antipolis, France.

DVORAK, G. J. and BAHEI-EL-DIN, Y. A. (1982) Plasticity analysis of fibrous composites. *J. Appl. Mech.* **49,** 327.

EGGLESTON, H. G. (1969) *Convexity*, p. 5. Cambridge University Press, Cambridge.

EISENBERG, M. A. and YEN, C. F. (1984) The anisotropic deformation of yield surfaces. *J. Engng Mater. Technol.* **106,** 355.

GURTIN, M. E. (1981) *An Introduction to Continuum Mechanics*, p. 229. Academic Press, New York.

HERSHEY, A. V. (1954) Plasticity of isotropic aggregates of anisotropic face centered cubic crystals. *J. Appl. Mech.* **76,** 241.

HILL, R. (1950) *The Mathematical Theory of Plasticity*. Clarendon Press, Oxford.
HILL, R. (1979) Theoretical plasticity of textured aggregates. *Math. Proc. Camb. Phil. Soc.* **85,** 179.
HILL, R. (1990) Constitutive modelling of orthotropic plasticity in sheet metals. *J. Mech. Phys. Solids* **38,** 405.
HOSFORD, W. F. (1972) A generalized isotropic yield criterion. *J. Appl. Mech.* **39,** 607.
HUTCHINSON, J. W. (1964) Plastic deformation of B.C.C. polycrystals. *J. Mech. Phys. Solids* **12,** 25.
KALIDINDI, S. R., BRONKHORST, C. A. and ANAND, L. (1992) Crystallographic texture evolution in bulk deformation processing of FCC metals. *J. Mech. Phys. Solids* **40,** 537.
KALLEND, J. S., KOCKS, U. F., ROLLET, A. D. and WENK, H.-R. (1989) popLA, The preferred Orientation Package from Los Alamos.
LEGE, D. J., BARLAT, F. and BREM, J. C. (1989) Characterization and mechanical modelling of the mechanical behavior and formability of a 2008-T4 sheet sample. *Int. J. Mech. Sci.* **31,** 549.
LIAN, J., BARLAT, F. and BAUDELET, B. (1989) Plastic behavior and stretchability of sheet metals. Part II: Effect of yield surface shape on sheet forming limit. *Int. J. Plasticity* **5,** 131.
LODE, W. (1926) Versuche ueber den Einfluss der mittleren Hauptspannung auf das Fliessen der Metalle Eisen Kupfer und Nickel. *Z. Physik.* **36,** 913.
MACEWEN, S. R., PERRIN, R. M., GREEN, D., MAKINDE, A. and NEALE, K. (1992) An evaluation of planar biaxial deformation in H19 can-stock sheet. *Proc. 13th RISO* (ed. S. J. ANDERSEN *et al.*), p. 539. Roskilde, Denmark.
MENDELSON, A. (1968) *Plasticity: Theory and Application*, p. 87. Macmillan, New York.
MISES, R. von (1913) *Gottinger Nachrichten, math. phys. klasse*, p. 582.
ONAT, T. (1981) Representation of inelastic behavior in the presence of anisotropy and finite deformations. *Plasticity of Metals at Finite Strain* (ed. E. H. LEE and R. L. MALLET).
ONAT, T. (1984) Effective properties of elastic materials that contain penny shaped voids. *Int. J. Engng Sci.* **22,** 1013.
RODIN, G. J. and PARKS, D. M. (1986) On constitutive relations in nonlinear fracture mechanics. *J. Appl. Mech.* **53,** 834.
SHIH, C. F. and LEE, D. (1978) Further developments in anisotropic plasticity. *J. Engng Mater. Technol.* **100,** 294.
STOUT, M. G., HECKER, S. S. and BOURCIER, R. (1983) An evaluation of anisotropic effective stress–strain criteria for the biaxial yield and flow of 2024 aluminum tubes. *J. Engng Mater. Technol.* **105,** p. 242.
TAYLOR, G. I. (1938) Plastic strains in metals. *J. Inst. Met.* **62,** 307.
TRESCA, H. (1864) *Comptes Rendus Acad. Sci.* **59,** 754.
TUCKER, G. E. C. (1961) Texture and earing in deep drawing of aluminum. *Acta Metall.* **9,** 275.
VOYADJIS, G. Z. and FOROOZESH, M. (1990) Anisotropic distortional yield model. *J. Appl. Mech.* **57,** 537.
WOODTHROPE, J. and PEARCE, R. (1970) The anomalous behavior of aluminum sheet under balanced biaxial tension. *Int. J. Mech. Sci.* **12,** 341.

APPENDIX 1: SYMMETRIES OF THE TRANSFORMATION TENSOR

As also shown by ONAT (1984), a fourth order tensor with the symmetries of (6) and (7) can be decomposed into a set of irreducible symmetric tensors:

$$L_{ijkl} = a\delta_{ij}\delta_{kl} + b(\delta_{ik}\delta_{jl} + \delta_{il}\delta_{jk}) + \delta_{ij}A_{kl} + A_{ij}\delta_{kl} + \delta_{ik}F_{jl} + \delta_{il}F_{jk} + \delta_{jk}F_{il} + \delta_{jl}F_{ik} + C_{ijkl} \qquad \text{(A1.1)}$$

where a and b are scalars, $\mathbf{A}$ and $\mathbf{F}$ are second order symmetric traceless tensors and $\mathbf{C}$ is a fourth order symmetric traceless tensor. However, by using the constraint of (8) we obtain

$$b = -\tfrac{3}{2}a,$$

$$\mathbf{F} = -\tfrac{3}{4}\mathbf{A}. \tag{A1.2}$$

Therefore, the final independent irreducible variables which compose $\mathbf{L}$ are a, $\mathbf{A}$ and $\mathbf{C}$. The decomposition of $\mathbf{L}$ according to (A1.1) and (A1.2) is unique. The form of the irreducible tensorial variables which compose $\mathbf{L}$ depends on the symmetry group of the considered material. When the material is symmetric then all components of $\mathbf{A}$ and $\mathbf{C}$ are zero. When the material is fully asymmetric then both $\mathbf{A}$ and $\mathbf{C}$ are fully developed.

Following ONAT's (1981) framework, we consider the irreducible variables a, $\mathbf{A}$ and $\mathbf{C}$ as state variables. These state variables can describe any desired material symmetry as tabulated in Table 1. The actual state of the material is represented by the set

$$\{Y, a, \mathbf{A}, \mathbf{C}, \sigma, \mathbf{B}\}. \tag{A1.3}$$

Introduction of additional irreducible tensors as state variables will not be considered here for a material that can exhibit only the groups of symmetries tabulated in Table 1.

Therefore the adopted form of $\mathbf{L}$ with the internal symmetries and constraints expressed by (6)–(8) is compatible with the use of only three irreducible variables for the state representation

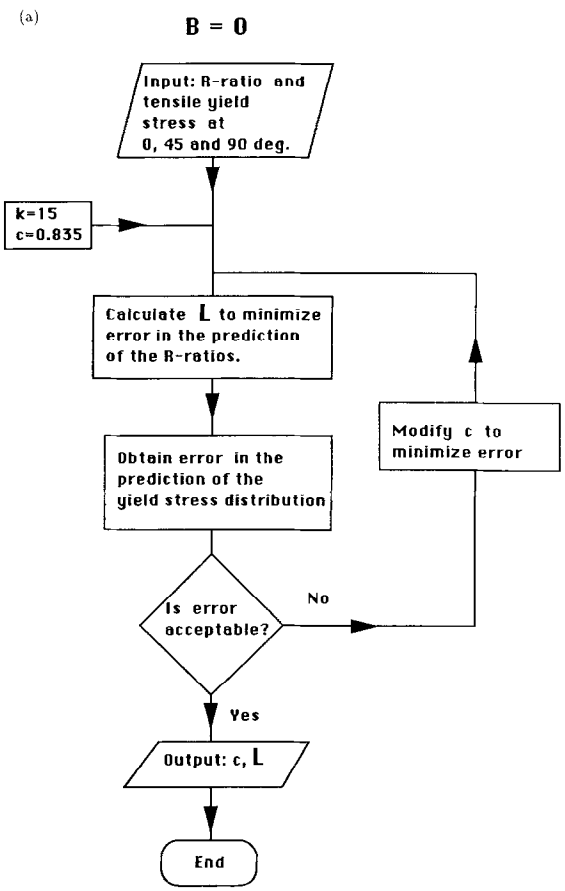

FIG. A2.1. (a) A flow chart of the numerical procedure used to calculate the yield surface when $\mathbf{B} = \mathbf{0}$. (b) A flow chart of the numerical procedure used to calculate the yield surface when $\mathbf{B} \neq \mathbf{0}$. *Continued overleaf.*

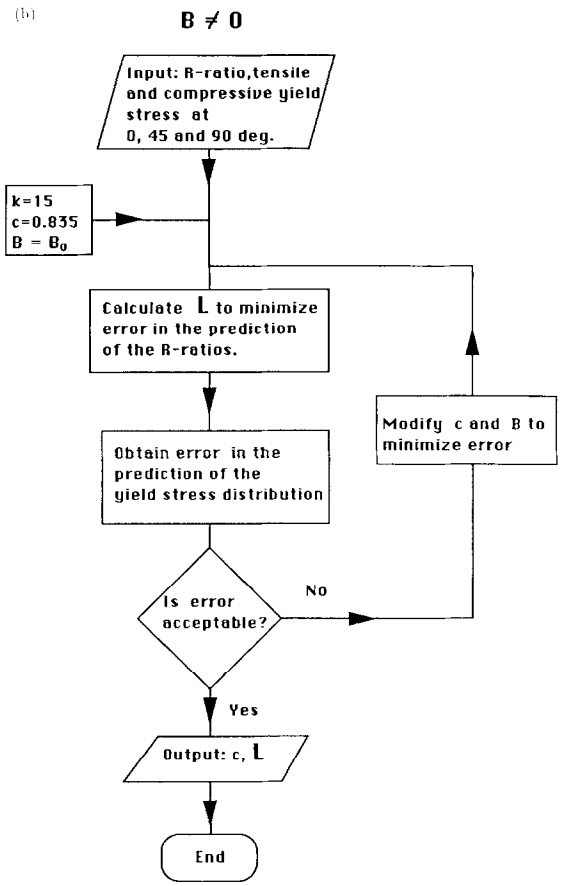

FIG. A2.1. *Continued.*

of the material anisotropy. However, (6) and (7) are the result of the symmetry of the stress tensor and the pressure independence of the yield condition, whereas (8) is artificially created in order to obtain the state representation of the anisotropy of the material with the minimal population of irreducible state variables.

APPENDIX 2: EVALUATION OF THE ANISOTROPY IN THE CASE OF ORTHOTROPIC SYMMETRY

We consider a thin rolled metallic sheet and an orthonormal reference frame $Oxyz$, where the x–y plane is in the plane of the sheet and the x-axis is along the rolling direction. Also, we concentrate on using the IPE yield function of (3) with the exponent k fixed to a high enough value ($k = 15$) to approximately describe the two bounds of the yield surface, whereas the mixing factor c will be determined to provide a best fit to the experimental data. As a first approximation we can use the value of c for isotropic materials, Method I, see Table 1.

If we assume orthotropic symmetry, then we can write (4) in a matrix form:

$$\begin{Bmatrix} S_x \\ S_y \\ S_z \\ S_{yz} \\ S_{zx} \\ S_{xy} \end{Bmatrix} = C \begin{bmatrix} 1 & \beta_1 & \beta_2 & . & . & . \\ \beta_1 & \alpha_1 & \beta_3 & . & . & . \\ \beta_2 & \beta_3 & \alpha_2 & . & . & . \\ . & . & . & \gamma_1 & . & . \\ . & . & . & . & \gamma_2 & . \\ . & . & . & . & . & \gamma_3 \end{bmatrix} \begin{Bmatrix} \sigma_x \\ \sigma_y \\ \sigma_z \\ \sigma_{yz} \\ \sigma_{zx} \\ \sigma_{xy} \end{Bmatrix} \tag{A2.1}$$

where all the blank components of the matrix representation of **L** in (A2.1) are zero. However, by using the pressure independence condition [equation (8)] we obtain:

$$\beta_1 = \frac{\alpha_2 - \alpha_1 - 1}{2}$$

$$\beta_2 = \frac{\alpha_1 - \alpha_2 - 1}{2}$$

$$\beta_3 = \frac{1 - \alpha_1 - \alpha_2}{2}. \tag{A2.2}$$

Therefore the tensorial operator consists of the following independent parameters:

$$\{C, \alpha_1, \alpha_2, \gamma_1, \gamma_2, \gamma_3\}.$$

For an isotropic material, we have:

$$C = \tfrac{2}{3}$$

$$\alpha_1 = \alpha_2 = 1$$

$$\gamma_1 = \gamma_2 = \gamma_3 = \tfrac{3}{2}. \tag{A2.3}$$

We consider stress states of the anisotropic material where the value of the out-of-plane shear stress is negligible (e.g. sheet forming processes). Also we assume that $\mathbf{B} = \mathbf{0}$. Thus, the values of γ_1 and γ_2 are not critical when describing the anisotropy of the material and are set equal to the corresponding isotropic values.

If $R(0)$, $R(90)$ are the measured R-ratios at 0° and 90° with respect to the rolling direction, we can show that $R(0)$, $R(90)$ are functions of only α_1, α_2. $R(0)$ and $R(90)$ can be calculated by straightforward use of (16). Therefore, we can calculate α_1, α_2 as the two unknowns in a system of two non-linear equations. For this purpose we used an error minimization numerical procedure (steepest gradient method).

In order to calculate the value of γ_3 we use the value of the R-ratio at 45° with respect to the rolling direction $R(45)$. By using (16) we can show that $R(45)$ is a function of α_1, α_2 and γ_3. Therefore, γ_3 can be obtained as a root of a non-linear equation, given that α_1, α_2 are already known.

We set now the value of the equivalent yield stress Y equal to the average yield stress as obtained by the three tension tests. We also require both the experimental and theoretical stress distributions in different directions in the plane of the sheet to have the same average value. However, by the homogeneity of the proposed yield function the averaged yield stress in the plane is inversely proportional to C. Therefore we can calculate C, as the ratio of the average experimental yield stress to the average yield stress obtained if we take $C = 1$.

Having calculated all the components of the IPE transformation tensor, we can predict the yield stress distribution and the yield surface. If experimental data for the yield stress distribution are available we can repeat the above described procedure with different values of c, until the error in the prediction of the yield stress distribution in different directions is minimized. Thus, we see that the necessary material parameters can easily be obtained through uniaxial tensile

tests only. A flow chart of the numerical procedure used to calculate the material parameters is shown in Fig. A2.1(a).

In the case where **B** is non-zero, the procedure remains virtually the same. In this case, both **B** and c must be modified in a closed loop towards the direction of steepest descent of the error of the predicted distribution of the tensile *and* compressive yield stress, until the error is minimized. A flow chart of the numerical procedure used to calculate the material parameters in this case is shown in Fig. A2.1(b).